ACS APPLIED MATERIALS & INTERFACES

Research Article

www.acsami.org

Hybrid-Type Quantum-Dot Cosensitized ZnO Nanowire Solar Cell with Enhanced Visible-Light Harvesting

Heejin Kim,[†,‡] Hyuncheol Jeong,[†,‡] Tae Kyu An,[§] Chan Eon Park,[§] and Kijung Yong*[,‡]

[‡]Surface Chemistry Laboratory of Electronic Materials (SCHEMA), Department of Chemical Engineering, and [§]POSTECH Organic Electronics Laboratory, Polymer Research Institute, Department of Chemical Engineering, Pohang University of Science and Technology (POSTECH), Pohang 790-784, Korea

Supporting Information

ABSTRACT: A polymer hybrid quantum-dot-sensitized solar cell was developed using CdSe/CdS/ZnO nanowires as a photoanode and regioregular P3HT as a conjugated polymer. The P3HT polymer was used as a hole transport material to replace the liquid electrolyte in quantum dot sensitized solar cells, CdSe/CdS acts as a cosensitizer, which enhances light harvesting in the visible range, and the ZnO nanowires provide a direct pathway for electron transport. Through an adequate cascade bandgap structure of the photoanode, the photo-excited electrons were effectively separated from the electron/hole pairs and transported under illumination. The remaining holes at the anode were transported by the conjugated polymer P3HT without any intermediate potential loss. The fabrication of the hybrid solar cell was optimized with various experimental conditions, including the length of the ZnO nanowires, quantum sensitizers, P3HT filling conditions, and electrolytes. The optimally obtained hybrid solar cells exhibited 1.5% power-conversion efficiency under AM 1.5G of 100 mW/cm^2 intensity. The fabricated hybrid cells exhibited highly durable cell performances, even after 1 month under atmospheric conditions, whereas the liquid junction quantum dot sensitized solar cells exhibited a significant degradation in their performances during the first 2 weeks immediately after fabrication. High open-circuit voltage and fill factor values of our hybrid quantum-dot-sensitized solar cell indicate that the applied hole transport layer efficiently dissociates electron/hole pairs at the interface and retards the interfacial charge recombination.

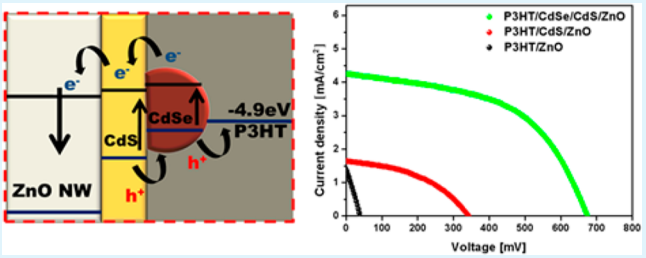

KEYWORDS: *hybrid, CdSe, CdS, ZnO, solar cell, nanowire*

1. INTRODUCTION

Recently, quantum-dot-sensitized solar cells (QDSSCs) have been the focus of considerable research attention because of their conceptual similarities with dye-sensitized solar cells (DSSCs) and the outstanding opto-electronic properties of quantum dot sensitizers.[1−3] Similar to DSSCs, QDSSCs generate excitons using specific visible light sensitizers and generally transport electrons to the counter electrodes through liquid-type electrolytes utilizing oxidation−reduction reactions. These distinguishing features greatly improve the ability of these cells to absorb sunlight, which results in increased photocurrents and cell performance. Particularly, versatile quantum dot sensitizers have great potential for photovoltaic applications because of their high absorption coefficient, tunable band gap energy (which is dependent on the size of the particle), and large intrinsic dipole moment.[4] Despite these advantages, QDSSCs generally exhibit low power conversion efficiency and a rapid decline of performance during operation. The presence of a liquid electrolyte in typical QDSSCs is one of the influential factors for these problems because it impedes the transport of electrons by forming an inefficient liquid−solid interface at the junction, it severely limits the open-circuit voltage, it induces a leakage current, and it photocorrodes the quantum dots.[5] For these reasons, p-type conjugated polymers have recently emerged as alternatives for the electrolyte because of their solid structure and ability to transport holes.

The concept of hybrid type solar cells, which consist of an n-type inorganic semiconductor and a p-type conjugated polymer, was first introduced to improve the performance of organic photovoltaics (OPVs) by forming hybrid mixtures of CdSe nanoparticles with organic materials.[6−10] The high electron affinity and mobility of CdSe cause it to function as an electron accepting and transporting material in OPVs. In addition to CdSe, large bandgap semiconductors such as ZnO and TiO_2, which can also accept and transport electrons through their conduction band, have begun to draw considerable attention for use as n-type electrodes in hybrid solar cells.[11−13] On the basis of these ZnO or TiO_2 electrodes, many research groups have recently succeeded in developing sensitized hybrid solar cells that utilize metal chalcogenide quantum dots, such as CdS,[14−17] CdSe,[8] PbS,[18] and Sb_2S_3.[19,20] However, the use of these quantum dot sensitizers has been mostly restricted to

Received: September 12, 2012
Accepted: December 11, 2012
Published: December 11, 2012

TiO_2 nanostructure-based electrodes,[21,22] and in many cases, only a single type of quantum dot has been used as the sensitizer;[23−25] therefore, the light harvesting was limited. To the best of our knowledge, ZnO nanowires cosensitized with CdS and CdSe have not been reported in semiconductor−polymer hybrid systems, despite the fact that liquid electrolyte-based solar cells with these multilayer sensitizers have been widely used as highly efficient photoanode structures.[15] Therefore, in this study, we have developed hybrid solar cells based on CdSe/CdS/ZnO nanowire arrays for the first time to overcome the aforementioned problems caused by a liquid electrolyte while simultaneously enhancing the harvesting of visible light when combined with a multilayer of CdSe/CdS quantum dots. Herein, the proposed hybrid system adopted a new hole transporting layer of conjugated polymer P3HT rather than a liquid electrolyte. This structure works as a p-i-n junction solar cell with a p-type polymer, a CdSe/CdS sensitizer, and n-type wide bandgap ZnO nanowires. The expected effect from this structure is a high open-circuit voltage due to its direct hole transport by the P3HT conjugated polymer, which lowers its potential loss. In addition, the efficient electron/hole pair dissociation can result in a higher fill factor. Under optimum fabrication conditions, the obtained hybrid solar cells exhibited a 1.5% light power-conversion efficiency under 1 sun illumination conditions and 4.2 mA/cm^2 (short circuit current), 675 mV (open circuit voltage), and a 51.8% fill factor. More importantly, the cell exhibited highly stable performances over 40 days, which is clearly superior to liquid electrolyte QDSSCs. This highly durable polymer based hybrid quantum dot sensitized solar cell has considerable potential for next generation solar cells.

2. EXPERIMENTAL SECTION

Fabrication of CdSe/CdS/ZnO Heterojunction Nanowire Arrays. CdSe/CdS/ZnO NW arrays were prepared using a three-step solution reaction method based on a previous report.[4] Arrays of ZnO NWs were grown on indium tin oxide (ITO) substrates (TEC, 8 Ω/sq.) using an ammonia solution method. A 50-nm-thick ZnO buffer film was sputtered on the ITO glass at room temperature. Then, the ZnO/ITO substrates were immersed in an aqueous solution containing 10 mmol of $Zn(NO_3)_2{\cdot}6H_2O$ and 2 mL of ammonium hydroxide solution (Sigma-Aldrich) in 100 mL of deionized water for 30 min ~2 h at 95 °C to grow the ZnO NW arrays. After calcination at 200 °C for 30 min, the ZnO NW arrays were sensitized in situ with CdS and CdSe using successive ionic layer adsorption and reaction (SILAR) and chemical bath deposition (CBD), respectively. The samples were dipped in 200 mM $CdSO_4$ for 30 s, rinsed with deionized water for 30 s, dipped for an additional 30 s in a 200 mM aqueous Na_2S solution, and then rinsed with water for 30 s. All of these processes constitute one SILAR cycle, and they were repeated for 10 cycles to obtain a suitable loading of CdS on the ZnO NWs. CdSe was deposited in situ on the CdS/ZnO NWs by CBD. The samples were immersed in an aqueous solution containing 0.5 mmol of $Cd(CH_3COO)_2$ $2H_2O$, 0.25 mmol of Na_2SeSO_3, and 150 μL of ammonium hydroxide solution in 20 mL of deionized water for 3 h at 95 °C. The samples were then annealed at the 200 °C for 1 h, and dried in a vacuum overnight before the deposition of P3HT.

Deposition of a Conjugated Polymer (P3HT). A layer of P3HT (Rieke Metals) was infiltrated into the CdSe/CdS/ZnO arrays by spin coating at 600 rpm for 30 s, followed by subsequent drying for 60 s at 2000 rpm in air from a P3HT solution (30 mg mL^{-1} in chlorobenzene). The samples were then annealed on a hot plate in a glovebox at 150 °C for 10 min followed by slowly cooling to room temperature. Finally, the Au electrodes with a thickness of 100 nm were thermally deposited in a vacuum (3 × 10^{-6} Torr). The evaporation was performed with a metal mask, which provided an active area of 16 mm^2 for each device.

Characterization. Scanning electron microscopy (SEM) images were recorded using a Phillips XL30S field emission SEM. An atomic scale analysis of the crystal structure was performed on a transmission electron microscope (JEM-2100F, JEOL) equipped with an energy-dispersive X-ray (EDX) spectrometer. The optical absorbance of the samples was analyzed using a UV2501PC (SHIMADZU) spectrometer with an ISR-2200 integrating sphere attachment for diffuse reflection measurements. The photocurrent density−voltage characteristics of the QDSSCs were measured under a simulated air mass 1.5 G solar spectrum. The intensity was adjusted to 100 mW/cm^2 using an NREL-certified silicon reference cell equipped with a KG-5 filter. The electrochemical impedance spectroscopy (EIS) measurements were performed using a Biologic SP-200 in the frequency range of 100 mHz to 100 kHz at open-circuit voltage.

3. RESULTS AND DISCUSSION

Figure 1a−d presents scanning electron microscope (SEM) images of the nanowire based hybrid structure according to the fabrication procedure. Figure 1a shows the bare ZnO nanowire arrays that were grown on the ITO substrate with a length of 800 nm and a diameter of 80−100 nm. The length of the ZnO nanowire was controlled by the duration growth time assisted by an ammonia solution. Subsequently, SILAR (successive ionic liquid absorption reaction) and CBD (chemical bath deposition) were performed to deposit the CdS and CdSe, respectively. Although there have been many attempts to coat of the quantum dots on the ZnO surface,[26,27] we employed SILAR process with in situ CdS synthesis.The SILAR process based on the successive surface adsorption of ions and thus enables the conformal coating of the quantum dots. The SILAR and CBD cycle numbers were controlled to obtain optimal

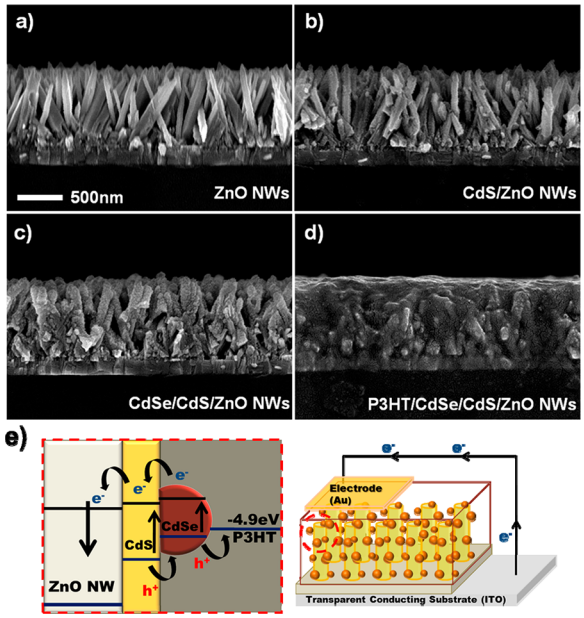

Figure 1. Cross-sectional SEM images of (a) bare ZnO NW arrays grown for 1 h at 95 °C using the CBD method, (b) CdS/ZnO NW arrays after 10 cycles of CdS SILAR, (c) CdSe/CdS/ZnO NW arrays after 3 h of CdSe CBD, and (d) CdSe/CdS/ZnO NW arrays infiltrated with P3HT by spin-coating. Here, all of the ZnO NWs were grown under the same conditions. (e) Energy structure diagram and schematic illustration of the Au/P3HT/CdSe/CdS/ZnO NW/ITO hybrid solar cell.

interspacing of the nanowire arrays for perfect infiltration of the P3HT. After the CdS and CdSe were deposited, the surface became rough and bumpy because of the CdS and CdSe particles (Figure 1b, c). In Figure 1b, the CdS/ZnO nanowire arrays revealed that ~9 nm of a CdS shell was uniformly coated over the entire ZnO nanowire surface after 10 cycles of the SILAR process. Therefore, the deposition of CdSe using the CBD process clearly generated the rougher surface of the nanowires. Finally, P3HT was infiltrated into the CdSe/CdS/ZnO nanowire arrays with ~100 nm overlayer thickness on the structure. These samples could also be distinguished by different colors observable with the naked eye (white, ZnO; yellow, CdS/ZnO; brown, CdSe/CdS/ZnO; and red-brown, P3HT infiltrated CdSe/CdS/ZnO). Figure 1e illustrates the basic structure and the overall operating mechanism of the proposed hybrid polymer solar cells based on the CdSe/CdS/ZnO nanowire arrays. With the illumination, the CdS and CdSe mainly absorb visible light, resulting in generation of the photoexcited electron−hole pairs. After that, the electrons that were photoexcited on the CdSe/CdS sensitizers were effectively transported to the ZnO nanowire through the cascade type-II band structure, whereas the remaining holes in the photoanode were transported through the P3HT hole transporting layer. The P3HT in this system acts as an excellent organic p-type charge transport materials with adequate HOMO level approximately −4.9 eV versus vacuum. The interface of P3HT and CdSe/CdS/ZnO operated with forming p-n heterojunction, which enables an efficient charge separation at the interface.[25] Unlike liquid junction QDSSCs, these hybrid type cells recover holes in the P3HT/photoanode interface rather than through a redox couple oxidation reaction of the electrolyte.

For the detailed surface morphological changes, transmission electron microscopy (TEM) was employed in order to examine the atomic structures of the deposited quantum dot semiconductor CdS and CdSe on the ZnO nanowire surface. After SILAR process for the CdS shell coating, the CdS shell layer was uniformly deposited on the ZnO nanowire surface (figure 2(a)). The HRTEM image taken from the interface region of the CdS/ZnO confirmed that polycrystalline CdS nanoparticles were deposited with 8−9 nm shell thickness after 10 cycles of SILAR process. The fast Fourier transform (FFT) patterns taken from the each part indicated that polycrystalline CdS shell layer was grown on the ZnO crystal nanowire. After CdSe CBD process, the surface morphological change was observed in TEM images of Figure 2c, d. In low-magnification TEM image of Figure 2c, the bumpy surface of heteronanostructures can be observed after CdSe deposition. HRTEM image in Figure 2d demonstrates that CdSe nanoparticle was deposited on the ZnO/CdS core/shell surface randomly. The FFT patterns taken from HRTEM image provide that crystal structure of CdSe/CdS/ZnO were formed with CBD, SILAR process. Also, spatial elemental analysis using electron energy loss spectroscopy (EELS) was examined with the CdSe/CdS/ZnO heteronanostructures. Figure 2e−i clearly shows that Zn is uniformly distributed along the core region and Cd, S, Se elements are found along the shell of the ZnO nanowire.

To investigate the light absorption properties, diffuse reflectance spectra (DRS) were obtained from identical samples as those of the SEM images. As observed in Figure 3, bare ZnO nanowire arrays (black line) exhibited absorption properties in the UV region that corresponded to its bandgap energy of ~3.4 eV. The ZnO nanowire arrays with deposited CdS, which are

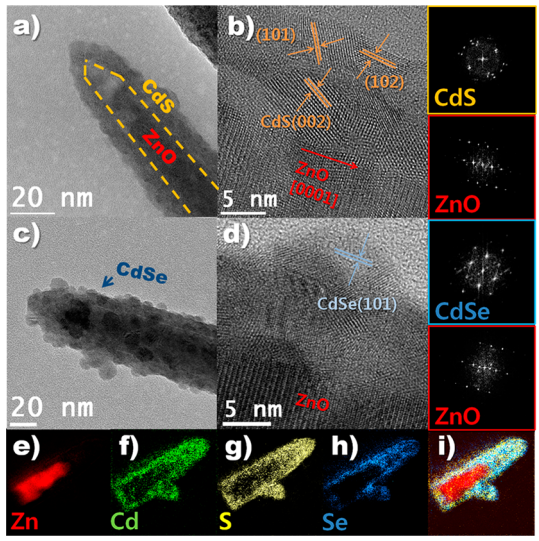

Figure 2. TEM images of (a, b) CdS/ZnO heterostructure nanowires and (c, d) CdSe/CdS/ZnO heteronanostructures nanowires: (a, c) low-magnification image and (b, d) a high-resolution TEM(HRTEM) image. The insets are FFT patterns of the CdS and ZnO obtained from b, and CdSe and ZnO obtained from d. (e, h) EELS elemental mapping images of the Zn,Cd,S, and Se, respectively. (i) Overlay EELS elemental mapping image of (e−h).

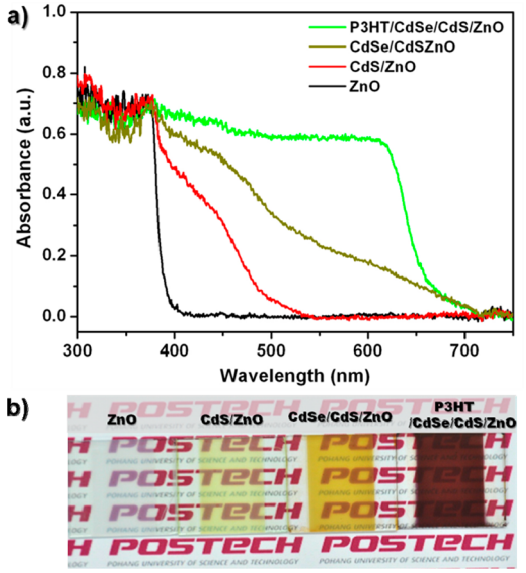

Figure 3. (a) Diffuse reflectance spectra (DRS) of as-prepared CdSe/CdS/ZnO NW arrays infiltrated with P3HT, CdSe/CdS/ZnO NW arrays, CdS/ZnO NW arrays, and ZnO NW arrays. (b) Digital image of identical samples on ITO substrate.

shown as a red line, exhibited red-shifted light absorption at a wavelength of ~500 nm, which was caused by the bandgap of 2.4 eV of the CdS shell. After deposition of CdSe onto the CdS/ZnO nanowires, the sample exhibited an onset of absorption at ~700 nm, which resulted from the 1.75 eV bandgap of CdSe. However, the infiltrated P3HT exhibited considerably enhanced light absorption over the range of visible light. It is believed that this enhancement is due to the adequate complemented absorption band created by the P3HT layer that has an absorption property at 400−650 nm and the CdSe/CdS layer. The absorption spectrum of P3HT/CdSe/CdS/ZnO effectively covers the visible light range of 400−700 nm, which

dx.doi.org/10.1021/am301960h | ACS Appl. Mater. Interfaces 2013, 5, 268−275

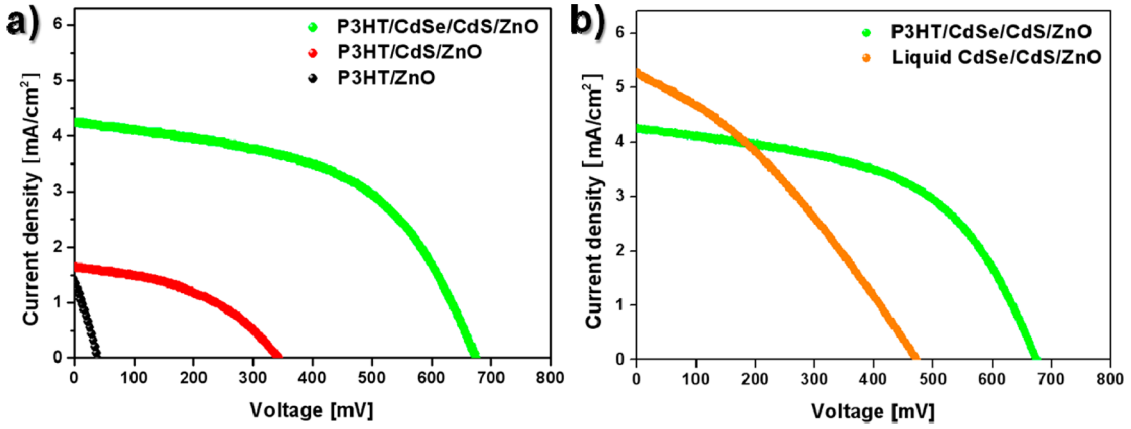

Figure 4. Illuminated (AM 1.5 G illumination at 100 mW/cm^2) I–V characteristics of (a) P3HT/ZnO NW hybrid devices with and without interface modifications employing CdS and CdSe QDs and (b) CdSe/CdS/ZnO NW-based devices employing different hole conductors, a polysulfide electrolyte, and P3HT, respectively. (Cell dimension 0.4 mm × 0.4 mm).

is not absorbed by bare ZnO nanowires. The color changes of the samples could be examined in digital photoimage of each sample having size 3.5 cm × 3.5 cm (Figure 3b).

We fabricated QDSSCs by depositing Au thin film electrodes on the various hybrid structures of P3HT/ZnO nanowires and measured their cell performances. Figure 4 compares the current density–voltage characteristics of different types of hybrid cells, P3HT infiltrated-ZnO, -CdS/ZnO, and -CdSe/CdS/ZnO under 1 sun (= 100 mW cm^{-2} AM1.5G solar illumination). Figure 4a clearly shows that the photovoltaic response from hybrid photovoltaic cells is greatly improved with the incorporation of the CdS and CdSe quantum dot sensitizer. The photovoltaic P3HT/CdSe/CdS/ZnO device yielded the highest efficiency of 1.5%, performance parameters are summarized in Table 1. The cell exhibits V_{oc}, J_{sc}, and FF

Table 1. *J*–*V* Curve Parameters Measured under 1 sun Illumination

sample	V_{oc}(mV)	J_{sc} (mA/cm^2)	FF	efficiency (%)	R_{shunt}(Ω)
P3HT/ZnO	40.6	1.3	27.5	0.02	161
P3HT/CdS/ZnO	341.3	1.6	43.4	0.24	2.70k
P3HT/CdSe/CdS/ZnO	675.2	4.2	51.8	1.50	4.11k
liquid CdSe/CdS/ZnO	470.7	5.3	32.8	0.82	658

values of 675.2 mV, 4.2 mA/cm^2, and 51.8%, respectively. The enhanced J_{sc} value of the sensitized cells compared to bare ZnO nanowires clearly reveals that the use of CdS and CdSe quantum dot sensitizers facilitates absorption of the entire visible spectrum region up to 700 nm. In addition, the open circuit voltage was drastically increased with the CdSe/CdS interlayer deposition, which resulted in a strong improvement in the device performance. This increase in the V_{oc} value can be explained according to three aspects. Previous reports have shown that the conduction band edge of CdS is 0.3 eV higher than that of ZnO,[28] and this band offset causes the acceptor work function to decrease after CdS modification on the ZnO surface. Consequently, the energy difference between the conduction band edge of the acceptor and the highest occupied molecular orbital (HOMO) of the P3HT increases, and higher V_{oc} values can be achieved. Modification with CdS and CdSe could also increase the V_{oc} value by passivating the surface states on the ZnO nanowires that may act as recombination or charge trapping sites.[29,30] This result can be demonstrated by analyzing the shunt resistance of the solar cells. The presence of shunt resistance prevents the photogenerated current from passing through internal defects that may provide an alternative path. Consequently, a low shunt resistance causes a decrease in the amount of current at the pn junction, fill factor, and voltage from the solar cell, and vice versa. As Table 1 shows, the interfacial modification of CdS and CdSe greatly improves the shunt resistance of the solar cell with the bare ZnO acceptor. This value was improved approximately 17 times after CdS modification, and further improvement was observed after coating CdSe on the CdS layer. Lastly, the increased carrier lifetime after the modification is another reason for the improved V_{oc} value.[29,30] As we can see in the band structure diagram of our solar cells (Figure 1e), the band structure of the ZnO/P3HT system becomes cascading after the insertion of the semiconductors with adequate band levels, CdS and CdSe. The cascading band structure increases the carrier lifetimes by effectively separating excitons at the junctions.[14,29,30] This conclusion is consistent with the analysis results from the EIS, which is shown later (Figure 6).

Furthermore, we have compared the performances of the hybrid cells with polysulfide liquid electrolyte based QDSSCs, as shown in Figure 4b. The liquid electrolyte based photovoltaic device was fabricated with Au sputtered counter electrode and polysulfide electrolyte (3:7 Methanol/DI water, 0.5 M Na_2S, 2 M S, and 0.2 M KCl). For comparison, CdSe/CdS/ZnO nanowire arrays prepared with the same growth conditions (75 min growth time, ~1 μm length) were used for both hybrid and liquid type QDSSCs cells. The reason for applying rather short length of ZnO nanowire (1 μm length) is due to poor filling of P3HT for longer nanowires array, which is also reported for a different type of solid-state electrolyte photovoltaic cell using spiro-OMeTAD.[31] In addition, a short length of ZnO nanowires is useful for the relatively short diffusion length of carriers in the polymer. Under this condition, the power conversion efficiency of the liquid electrolyte QDSSC was lower than that of the hybrid photovoltaic system. As observed in Figure 4b, the current density of the liquid junction solar cell was higher than that of the hybrid cell because of its characteristic chemical cell that uses redox couples. Additionally, a possible reason for the low current density of the hybrid cell could be the relatively low

dx.doi.org/10.1021/am301960h | ACS Appl. Mater. Interfaces 2013, 5, 268–275

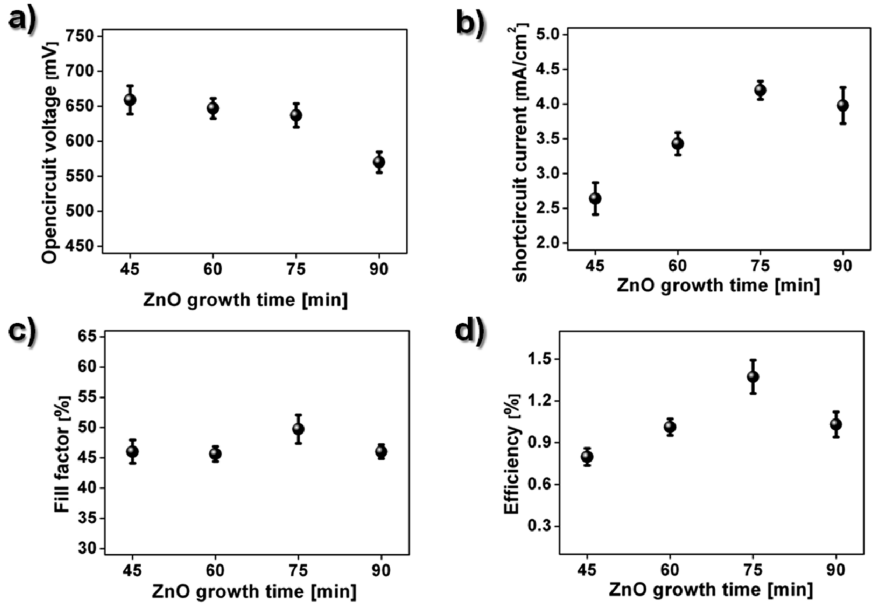

Figure 5. Illuminated $I-V$ characteristics of P3HT/CdSe/CdS/ZnO nanowire with ZnO NW growth time. Here, the ZnO NWs were grown for 1 h at 95 °C using the CBD method under identical conditions.

Table 2. $J-V$ Curve Parameters under 1 sun Illumination with Different ZnO NW Growth Times

sample	V_{oc}(mV)	J_{sc}(mA/cm^2)	FF	efficiency(%)
growth time 45 (631 nm ± 18 nm)	667(± 17.0)	2.58 (± 0.21)	46 (± 1.93)	0.8 (± 0.06)
growth time 60 (775 nm ± 6.6 nm)	657 (± 16.3)	3.45 (± 0.19)	46 (± 1.24)	1.0 (± 0.06)
growth time 75 (1.0 μm ± 44 nm)	651 (± 29.3)	4.23(± 0.12)	50 (± 2.35)	1.4 (± 0.12)
growth time 90 (1.45 μm ± 53 nm)	561 (± 21.3)	4.14 (± 0.13)	46 (± 1.14)	1.0 (± 0.09)

charge mobility of the P3HT hole conductor. Compared to the liquid electrolyte (1×10^{-2} to 1×10^{-1} cm^2 V^{-1} s^{-1}), P3HT exhibits a relatively low carrier mobility of 10^{-5} ~1×0^{-3} cm^2 V^{-1} s^{-1} in field effect transistors.[6] For this reason, P3HT provides lower hole-collection efficiency than that of liquid based devices, which could lead to an excessive interfacial recombination loss.[32] However, the open circuit voltage of the hybrid cell was higher than that of the liquid photovoltaic system. This result would reflect that a high potential loss occurs in the liquid redox couple electrolyte with an intermediate potential gap. In the case of the sensitized solar cells that use the liquid electrolyte, they require an additional overpotential to regenerate the oxidized sensitizer (0.2−0.3 eV).[33−35] However, the hole transfer directly occurs from the oxidized sensitizer to the HOMO level of the hole conductor in the hybrid cell. Therefore, the output voltage of the hybrid system is largely dependent on the difference between the electron quasi-Fermi level in the photoanode under illumination and the HOMO level of the P3HT. In case of P3HT, the HOMO level is located at −4.9 eV[36] and the donor level of polysulfide is estimated to be located at −4.0 eV.[37] In other words, the calculated potential gap of the P3HT hybrid device is higher compared to that of the conventional polysulfide electrolyte. This suggestion can explain the enhanced open circuit voltage value. The obtained parameters of Figure 4a, b are summarized in Table 1.

The effects of the length of the ZnO nanowires on the performances of the cells were also investigated, and the results are shown in Figure 5. For a more accurate comparison, we have performed repeated experiments for the fabrication and measurement of the cell performances. The averaged cell performance parameter values are summarized in Table 2. Except for the length of the ZnO nanowires, the other conditions of the cell fabrication were fixed including the sensitizer loading, the P3HT filling, and the counter electrode deposition. Figure 5a indicates that the current density (J_{sc}) is clearly related to the length of the ZnO nanowire. The current density increased with an increasing length of the ZnO nanowire but became saturated beyond 75 min of growth time for ZnO nanowires, which corresponds to ~1 μm in length. With increasing nanowire length, the amount of loaded quantum dots (CdS, CdSe) will be increased due to the increase of the ZnO surface area. However, when the nanowire length is too long (greater than 1 μm), the infiltration of P3HT through the CdSe/CdS/ZnO NW arrays becomes difficult, and this imperfect interface can cause increased electron recombination. In the case of V_{oc}, on the other hand, it decreases slightly with increasing length of the ZnO nanowire and then drops when the length of the nanowire is greater than 1 μm (Figure 5b). This dependence of V_{oc} on the nanowire length can be interpreted by two factors; the increased recombination sites and restricted charge transport in longer nanowire arrays. Longer nanowires provide greater surface area that has higher surface states and could also retard charge transport through hole transporting materials that have low mobility. The fill factors do not show any noticeable dependence on the length of the nanowire. Combining these parameters, the overall cell efficiency was enhanced with increasing nanowire length; it reached an average value of 1.4% (maximum ~1.5%) with a nanowire length of ~1 μm. Above this length, the efficiency decreases, which is due to the decrease of V_{oc}. These results are summarized in Table 2.

In this study, the hybrid solar cells of the CdSe/CdS cosensitized ZnO nanowires with P3HT exhibited the best photovoltaic performance among several different structures of hybrid cells. Compared to CdS sensitized ZnO nanowires (0.24%), the conversion efficiency of the cell dramatically increased to 1.5%. For a better understanding of the origin of the observed enhancement in the device performance after the deposition of CdSe, we utilized electrochemical impedance spectroscopy (EIS) and dark $I-V$ measurements. EIS is a steady state method for measuring the current response to the application of an AC voltage as a function of the frequency. EIS is used for evaluating the charge transfer rate at the interface of either the photoanode/HTM(P3HT) or HTM/CE. The EIS measurement was conducted in dark conditions at the open circuit voltage with a frequency ranging from 0.1 to 100 kHz. In our measurement, one semicircle was observed in the Nyquist plots for each cell (Figure 6). The semicircle in the Nyquist

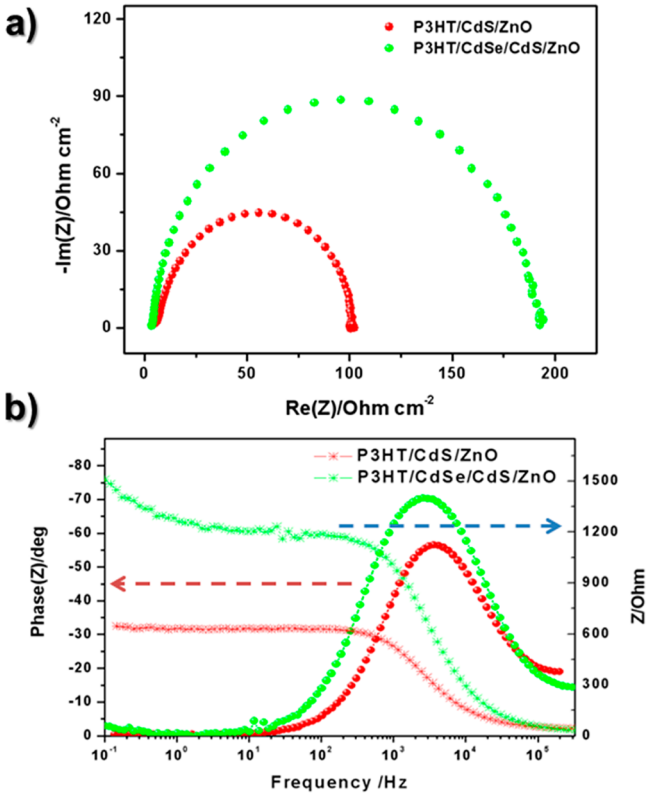

Figure 6. Electrical impedance spectra: (a) Nyquist plot of P3HT/CdS/ZnO NW and P3HT/CdSe/CdS/ZnO NW hybrid solar cells at the open circuit bias in the dark condition, (b) Bode impedance plot of corresponding samples.

plot is associated with charge transfer to the ZnO nanowire electrode, backward charge transfer from the ZnO nanowire electrode to the hole transport materials (P3HT), and the overall chemical capacitance.[38] In particular, the semicircle in the Nyquist plots corresponding to a middle frequency region is attributed to the electron transfer at the ZnO/CdS/CdSe/P3HT interface layer. In our system, the larger semicircle was observed in the dark condition, which is related to the electron recombination resistance.[39,40] In Figure 6a, the larger arc size of the P3HT/CdSe/CdS/ZnO sample indicates that its recombination resistance is greater than that of the P3HT/CdS/ZnO based device. The larger recombination resistance means that the device has a lower recombination rate than that of the sample with no CdSe. In the bode-plots (Figure 6b), the peak frequency was shifted to a lower value after the deposition of CdSe, which indicates that the CdSe modified hybrid device not only lowers the transport resistance but also results in a higher electron lifetime compared to the sample with no CdSe. Furthermore, the electron lifetime (τ) can be evaluated using the relation $\tau = 1/2\pi f_{mid}$, where f_{mid} is the midfrequency peak of the bode phase plots (Figure 6b) in the impedance spectra.[41] The calculated electron lifetime (τ) was 44 μs for the CdS/ZnO NW hybrid cell and 62 μs for the CdSe/CdS/ZnO NW hybrid cell. These results are consistent with EIS analysis results of Figure 6a. In addition, these results can explain the higher open circuit voltage of the CdSe modified hybrid solar cell, which is caused by longer electron lifetime values. For further investigation, the dark $J-V$ measurements were conducted with the corresponding samples. The dark current in solar cells primarily results from the recombination/interfacial trap and electron leakage current at the interface of the heterojunction.[42] In the dark $J-V$ curves (Figure 7), the dark current density

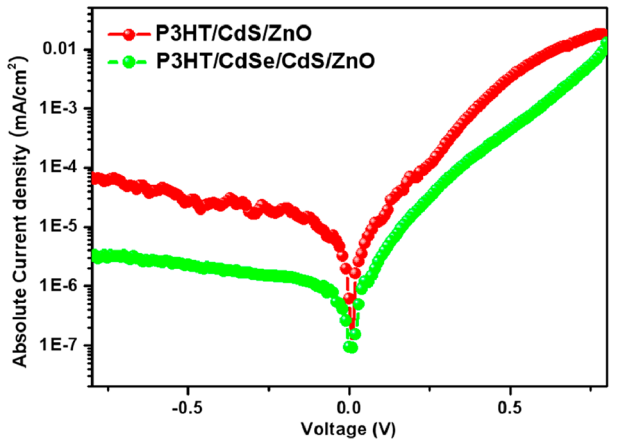

Figure 7. Dark $J-V$ measurement of the P3HT based hybrid device with different photoanodes; (red dot) P3HT/CdS/ZnO NW and (green dot) P3HT/CdSe/CdS/ZnO.

decreased after deposition of CdSe onto the CdS/ZnO nanowire arrays. At reverse bias, the P3HT/CdSe/CdS/ZnO NW device exhibited a lower leakage current compared to the P3HT/CdS/ZnO NW device, which suggests that less recombination occurs because of the presence of the CdSe layer. In addition, the smaller dark current density in the forward bias indicates that the CdSe modified device has fewer recombination sites and interfacial traps. On the basis of these results, the P3HT/CdSe/CdS/ZnO NW device not only exhibits efficient light harvesting but also a low recombination rate with a high electron lifetime.

Figure 8 shows the incident photon-to-current efficiency (IPCE) of the P3HT/CdS/ZnO and P3HT/CdSe/CdS/ZnO nanowire device as a function of the wavelength measured under short circuit conditions. In P3HT/CdS/ZnO, the IPCE spectrum shows a large, broad peak centered around 400−550 nm, which comes from the CdS and P3HT. Especially, around 450 nm a broad peak originating from the photocurrent generated in CdS can be observed. After CdSe deposition, the P3HT/CdSe/CdS/ZnO showed relatively high IPCE intensity than that of the P3HT/CdS/ZnO. In P3HT/CdSe/CdS/ZnO system the IPCE spectrum exhibits a photoresponse over the

dx.doi.org/10.1021/am301960h | ACS Appl. Mater. Interfaces 2013, 5, 268−275

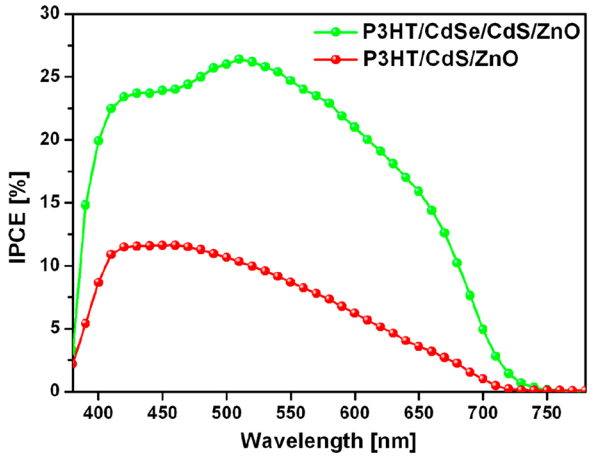

Figure 8. Incident photon-to-current conversion efficiency (IPCE) spectrum of P3HT/CdSe/CdS/ZnO NW solar cell.

entire visible-light range of 350−700 nm and shows a maximum IPCE of ∼25% at a wavelength of 530 nm.

This result clearly reveals that the CdSe/CdS cosensitized ZnO nanowire enables utilization of long-range visible light. In particular, maximum IPCE values in the 450−650 nm range are attributed to the contribution from the P3HT hole conductor providing visible-light absorption, efficient charge separation, and transport through the adequate band structure with the photoanode.

Another strong point of this hybrid system is its high durability of the device performances compared to that of liquid junction solar cells. In general, liquid junction solar cells are struggling from the low stability due to the corrosion of quantum dots, leakage currents, and side reactions at the electrolyte/counter electrode interface. In this respect, hybrid solar cells have advantages such as nonvolatility, robustness to corrosion, and air stability.[40,43] Figure 9 shows the cell performance durability for 40 days. The hybrid cell performance was measured every 8 days with air, and the results indicated that it was not degraded even after 40 days. However, the liquid junction solar exhibited a drastic degradation in performance within two weeks after fabrication. The dependence of the current density on time durations exhibited considerable differences between the two cells; the J_{sc} value of the liquid junction solar cell decreased more than 50%, whereas the J_{sc} value of the hybrid solar cell decreased by only 10%. The open circuit voltage was enhanced after 40 days in the hybrid cells, which is due to its improved interfacial contact and crystallinity, and the evaporation of the remaining solvent. Fill factor was not much affected by time duration and the overall conversion efficiency was decreased by only ∼5% after 40 days. This high stability in the cell performances of our hybrid QDSSCs exhibits a good potential as a next-generation solar cell.

4. CONCLUSIONS

In conclusion, a CdSe/CdS cosensitized ZnO NW hybrid solar cell with P3HT was developed and characterized in this research. The ZnO nanowire offers a one-dimensional electron pathway for the efficient transfer of electrons, and the CdSe/CdS resulted in efficient visible light harvesting through an adequate band structure. The photogenerated electron/hole pairs were effectively separated by the conjugated polymer P3HT. In the hybrid system, the optimally fabricated P3HT/CdSe/CdS/ZnO nanowire solar cells exhibited approximately 1.5% efficiency under 1 sun illumination. Specifically, the hybrid system exhibited an enhanced open circuit voltage value, which indicates that the hole transport material offers a low loss in potential in the solar cell system. The fabricated hybrid cell exhibited remarkable durability in cell performance; the cell efficiency decreased by only a few percent in air over 40 days. These results indicate that the conjugated P3HT polymer in our CdSe/CdS/ZnO nanowire system can offer highly stable cell performances compared to that of liquid-based, quantum-dot-sensitized solar cells.

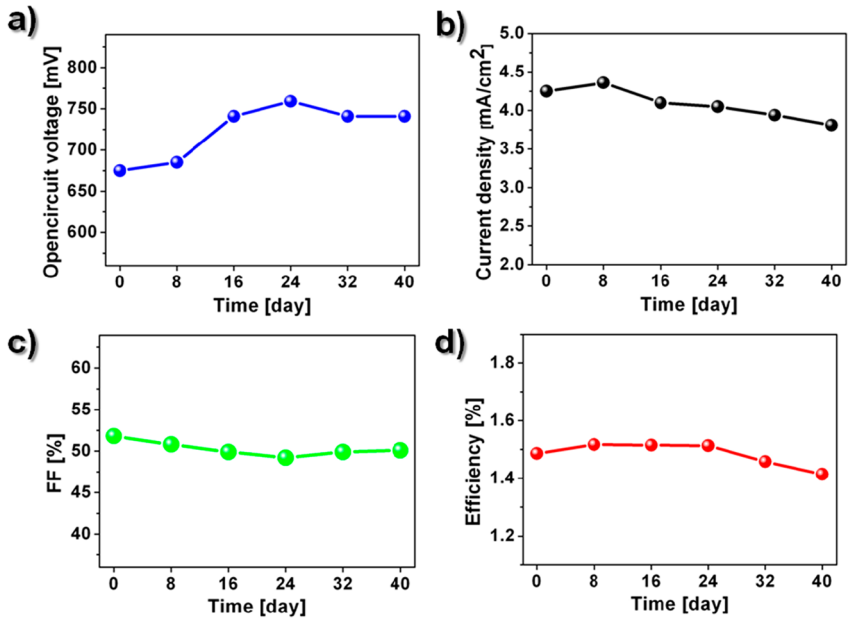

Figure 9. Stability tests of (a) current density, (b) open circuit voltage, (c) fill factor, and (d) cell efficiency as a function of time for the Au/P3HT/CdSe/CdS/ZnO NW/ITO device stored for 40 days in air under ambient conditions.

■ ASSOCIATED CONTENT

Supporting Information

Additional figures (PDF). This material is available free of charge via the Internet at http://pubs.acs.org.

■ AUTHOR INFORMATION

Corresponding Author

*E-mail: kyong@postech.ac.kr. Phone: +82-54-279-2278.

Author Contributions

†These authors contributed equally to this article.

Notes

The authors declare no competing financial interest.

■ ACKNOWLEDGMENTS

This work was supported by grants from the National Research Foundation (NRF2010-0009545) and by the Korea Research Foundation Grants funded by the Korean Government (MOEHRD) (KRF-2008-005-J00501)and Hyundai-Kia Motors.

■ REFERENCES

(1) Lee, Y. L.; Lo, Y. S. *Adv. Funct. Mater.* **2009**, *19*, 604.
(2) Lee, Y. L.; Huang, B. M.; Chien, H. T. *Chem. Mater.* **2008**, *20*, 6903.
(3) Kamat, P. V. *J. Phys. Chem. C.* **2008**, *112*, 18737.
(4) Seol, M.; Kim, H.; Tak, Y.; Yong, K. *Chem. Commun.* **2010**, *46*, 5521.
(5) Ruhle, S.; Shalom, M.; Zaban, A. *Chemphyschem* **2010**, *11*, 2290.
(6) Huynh, W. U.; Dittmer, J. J.; Alivisatos, A. P. *Science* **2002**, *295*, 2425.
(7) Liu, J. S.; Tanaka, T.; Sivula, K.; Alivisatos, A. P.; Frechet, J. M. J. *J. Am. Chem. Soc.* **2004**, *126*, 6550.
(8) Sun, B. Q.; Marx, E.; Greenham, N. C. *Nano Lett.* **2003**, *3*, 961.
(9) Huynh, W. U.; Peng, X. G.; Alivisatos, A. P. *Adv. Mater.* **1999**, *11*, 923.
(10) Gur, I.; Fromer, N. A.; Chen, C. P.; Kanaras, A. G.; Alivisatos, A. P. *Nano Lett.* **2007**, *7*, 409.
(11) Baeten, L.; Conings, B.; Boyen, H. G.; D'Haen, J.; Hardy, A.; D'Olieslaeger, M.; Manca, J. V.; Van Bael, M. K. *Adv. Mater.* **2011**, *23*, 2802.
(12) Greene, L. E.; Law, M.; Yuhas, B. D.; Yang, P. D. *J. Phys. Chem. C.* **2007**, *111*, 18451.
(13) Olson, D. C.; Lee, Y. J.; White, M. S.; Kopidakis, N.; Shaheen, S. E.; Ginley, D. S.; Voigt, J. A.; Hsu, J. W. P. *J. Phys. Chem. C.* **2007**, *111*, 16640.
(14) Zhong, M.; Yang, D.; Zhang, J.; Shi, J.; Wang, X.; Li, C. *Sol. Energy Mater. Sol. Cells* **2012**, *96*, 160.
(15) Jiang, X.; Chen, F.; Weiming, Q.; Yan, Q.; Nan, Y.; Xu, H.; Yang, L.; Chen, H. *Sol. Energy Mater. Sol. Cells* **2010**, *94*, 2223.
(16) Lee, Y. H.; Im, S. H.; Chang, J. A.; Lee, J. H.; Seok, S. I. *Org. Electron.* **2012**, *13*, 975.
(17) Wu, S.; Li, J.; Lo, S.-C.; Tai, Q.; Yan, F. *Org. Electron.* **2012**, *13*, 1569.
(18) Plass, R.; Pelet, S.; Krueger, J.; Gratzel, M.; Bach, U. *J. Phys. Chem. B* **2002**, *106*, 7578.
(19) Chang, J. A.; Rhee, J. H.; Im, S. H.; Lee, Y. H.; Kim, H. J.; Seok, S. I.; Nazeeruddin, M. K.; Gratzel, M. *Nano Lett.* **2010**, *10*, 2609.
(20) Cardoso, J. C.; Grimes, C. A.; Feng, X. J.; Zhang, X. Y.; Komarneni, S.; Zanoni, M. V. B.; Bao, N. Z. *Chem. Commun.* **2012**, *48*, 2818.
(21) Kamat, P. V. *Acc. Chem. Res.* **2012**, DOI: 10.1021/ar200315d.
(22) Zhang, Q.; Guo, X.; Huang, X.; Huang, S.; Li, D.; Luo, Y.; Shen, Q.; Toyoda, T.; Meng, Q. *Phys. Chem. Chem. Phys.* **2011**, *13*, 4659.
(23) Sun, B.; Hao, Y.; Guo, F.; Cao, Y.; Zhang, Y.; Li, Y.; Xu, D. *J.Phys.Chem.C* **2011**, *116*, 1395.
(24) Heo, J. H.; Im, S. H.; Kim, H.-j.; Boix, P. P.; Lee, S. J.; Seok, S. I.; Mora-Seró, I.; Bisquert, J. *J. Phys. Chem. C* **2012**, *116*, 20717.
(25) Hao, Y.; Pei, J.; Wei, Y.; Cao, Y.; Jiao, S.; Zhu, F.; Li, J.; Xu, D. *J.Phys.Chem.C* **2010**, *114*, 8622.
(26) Kim, J. Y.; Osterloh, F. E. *J. Am. Chem. Soc.* **2005**, *127*, 10152.
(27) Zeng, T.-W.; Liu, I. S.; Huang, K.-T.; Liao, H.-C.; Chien, C.-T.; Wong, D. K.-P.; Chen, C.-W.; Wu, J.-J.; Chen, Y.-F.; Su, W.-F. *J. Colloid Interface Sci.* **2011**, *358*, 323.
(28) Ruckh, M.; Schmid, D.; Schock, H. *J. Appl. Phys.* **1994**, *76*, 5945.
(29) Spoerke, E. D.; Lloyd, M. T.; McCready, E. M.; Olson, D. C.; Lee, Y. J.; Hsu, J. W. P. *App.Phys.Lett.* **2009**, *95*, 213506.
(30) O'Regan, B. C.; Scully, S.; Mayer, A. C.; Palomares, E.; Durrant, J. *J. Phys. Chem. B* **2005**, *109*, 4616.
(31) Chi, C.-F.; Chen, P.; Lee, Y.-L.; Liu, I. P.; Chou, S.-C.; Zhang, X.-L.; Bach, U. *J. Mater. Chem.* **2011**, *21*, 17534.
(32) Zhang, W.; Cheng, Y.; Yin, X.; Liu, B. *Macromol. Chem. Phys.* **2011**, *212*, 15.
(33) Boschloo, G.; Hagfeldt, A. *Acc. Chem. Res.* **2009**, *42*, 1819.
(34) Hardin, B. E.; Snaith, H. J.; McGehee, M. D. *Nat. Photonics* **2012**, *6*, 162.
(35) Snaith, H. J. *Adv. Funct. Mater.* **2010**, *20*, 13.
(36) Zeng, T.-W.; Liu, S.; Hsu, F.-C.; Huang, K.-T.; Liao, H.-C.; Su, W.-F. *Opt. Express* **2010**, *18*, A357.
(37) Fabregat-Santiago, F.; Garcia-Belmonte, G.; Mora-Sero, I.; Bisquert, J. *Phys. Chem. Chem. Phys.* **2011**, *13*, 9083.
(38) Leever, B. J.; Bailey, C. A.; Marks, T. J.; Hersam, M. C.; Durstock, M. F. *Adv. Ener. Mater.* **2012**, *2*, 120.
(39) González-Pedro, V.; Xu, X.; Mora-Seró, I.; Bisquert, J. *ACS nano* **2010**, *4*, 5783.
(40) Kern, R.; Sastrawan, R.; Ferber, J.; Stangl, R.; Luther, J. *Electrochim. Acta* **2002**, *47*, 4213.
(41) Wang, H.; Liu, G.; Li, X.; Xiang, P.; Ku, Z.; Rong, Y.; Xu, M.; Liu, L.; Hu, M.; Yang, Y. *Energy Environ. Sci.* **2011**, *4*, 2025.
(42) Musselman, K. P.; Marin, A.; Schmidt-Mende, L.; MacManus-Driscoll, J. L. *Adv. Funct. Mater.* **2012**, *22*, 2202.
(43) Reeja-Jayan, B.; Manthiram, A. *Sol. Energy Mater. Sol. Cells* **2010**, *94*, 907.